Journal of Hydroscience and Hydraulic Engineering
Vol. 1, No. 2, November, 1983, pp.33-51.

INITIAL ENTRAINMENT AND LATERAL SPREAD OF THREE-DIMENSIONAL BUOYANT SURFACE JET

By

Akira Murota

Department of Civil Engineering, Osaka University, Osaka 565, Japan

Kohji Muraoka

Hydrospheric Environmental Management Section, National Institute for Environment Studies, Yatabe, Ibaraki 305, Japan

and

Keiji Nakatsuji

Department of Civil Engineering, Osaka University, Osaka 565, Japan

SYNOPSIS

Spread of three-dimensional buoyant surface jets with small densimetric Froude numbers is studied experimentally by means of measurements of velocity and excess-concentration profiles and flow-visualization techniques of surface flow patterns. The modified theory using the entrainment velocity is developed according to the similarity of velocity distribution, and the mechanism of entrainment might be explained by the predicted volume entrained vertically and horizontally. Furthermore, the characteristics of streamlines, streaklines and particle paths at the water surface are helpful to reveal the buoyancy effects upon the entrainment and the lateral spread. The experimental results show that the buoyancy counteracts the vertical entrainment to form a thin surface layer like a horizontal plane jet. The lateral spread is enlarged, thereby, accompanied with horizontal entrainment and increase of the density difference. This lateral spread due to the buoyancy alone can be explained in terms of the density-induced front motion of buoyant discharges.

INTRODUCTION

In view of the increase of thermal waste water coupled with the rapid increase in electric-power demand, the continuous monitoring of changes in the water environment is necessary. Three basic engineering systems are used for the treatment of thermal waste water from a power plant : the surface discharge, the submerged discharge and the cooling tower. They have merits and demerits, but surface discharge seems to have lower cost in general, taking account of the large size of power plants. However, as such a discharge affects a broad region of water, accurate and careful planning is necessary in the design of the effluent works and the prediction of water temperatures.

In the last twenty years there has been remarkable progress in research on buoyant surface jets, and its results have been successfully reflected in mathematical modeling, among those are Tamai, Wiegel and Tornberg (22), Stefan and Vaidyaraman (19), Hayashi and Shuto (10), Tamai (21), Stolzenbach and Harleman (20) and Dunn, Policastro and Paddock (7). Recent developments of theoretical analyses and hydraulic experiments are minutely reviewed by Muraoka and Nakatsuji (15). These researches have been studied in the extension of a free turbulent jet. As the problems involved are three dimensional, it is necessary to investigate the buoyancy effects upon the vertical entrainment, the lateral spread and the pressure

distribution in the jet.

It is convenient to consider the cooling of a surface discharge separately in two distinct region : the near field and the far field. In the near field, which is called the *initial mixing region*, the momentum flux of the effluent water body forms itself into a prevailing jet flow from the outfall. The total sectional flow rate rapidly increases downstream in this field because of dominant entrainment from both lateral and lower water bodies with irregular eddy motions, and there is a rapid decrease in the difference in velocity and density between the jet flow and the ambient water. In the far field, called the *off-shore diffusion region*, the initial momentum of the jet is dispersed in space and hence the discharged water body gradually loses the characteristics of a jet and becomes a mild density current. In that process, the effluent water spread thinly over a tongue-like region, in such a manner that it develops the lateral mixing due to the horizontal turbulent eddies in the water region, while no vertical mixing occurs.

The near field behaviors are of particular interest because the size and character of buoyant discharges in the far field depend on the amount of near field mixing itself. In the near field, outfall structures must design their discharges to meet regulation criteria of mixing zone. Moreover, the near field is the region of great interest from a viewpoint of biological performance. In spite of these importance, three-dimensional experiments in the near field have been hardly carried out to gain a clear understanding of entrainment, although there were some experiments to measure profiles of velocity and temperature for verifying mathematical models.

The phenomena being important to the near field behavior of buoyant surface jets are (i) reduction of the vertical entrainment and (ii) lateral gravitational spread, which are markedly different from a homogeneous surface jet. The indirect effect of buoyancy (i) that counteracts the vertical entrainment has been experimentally studied by many investigators such as Ellison and Turner (8) and Asaeda and Tamai (3). They proposed good empirical formulae between the vertical entrainment velocity and the overall Richardson number for the case of two-dimensional stratified shear flows. On the other hand, experimental and theoretical researches on the lateral spread (ii) are scarce. Only Hayashi and Shuto (11) and Stefan et al. (18) recently investigated the process of the lateral spread in the near field. At present, a treatment of the near field zone in most mathematical models is still left obscure and is based on numerous untested assumptions because of lack of adequate information of physical process.

For this reason, fundamental experiments were carried out to obtain a physical understanding of three-dimensional buoyant surface jets with rather small densimetric Froude numbers. The process of the initial entrainment and the lateral spread in the near field was investigated. This paper is composed of two experiments : measurements of velocity and excess-concentration and flow-visualization of surface flow patterns. In the former, the modified theory using the entrainment hypothesis was developed based on measured velocity and excess-concentration distributions. The predicted volumes entrained vertically and horizontally were compared with the experimental data. Second, in the latter, the mechanism of the lateral spread was clarified based on the flow patterns at the water surface. The information obtained through the present study can be great importance to provide a realistic picture of downstream flow field of buoyant surface discharge.

EXPERIMENTAL SETUP AND PROCEDURE

The experiments were carried out in two hydraulic basins ; a 12.0 m long, 6.0 m wide, and 0.7 m deep one for series A, and a 3.0 m long, 1.5 m wide, and 1.5 m deep one for series B. These basins were initially filled up with salt water. Fresh water was discharged over a quiescent saline water ambient from an outfall of a rectangular channel placed at the center of short side, and the overflow was provided at the opposite side. In order to keep the outfall depth constant, discharged fresh water was siphoned over through 13 vinyl tubes equipped 1.0 cm beneath the water surface at the downstream side of the basin during a cource of experiment. Because of the limited volume of the basin, it is impossible to

preserve an experiment steady for a long time. Soon after the continuous discharge of fresh water was started, a horizontal large circulation was formed on both sides of the jet in some cases. Hence, measurements had to be made during only a few minutes after an establishment of the quasi-steady state was confirmed by observation of surface flow pattern. This state was also checked from the vertical profile of concentration measured by a salino-meter.

The density was measured with salino-meters each of which has a detector with a platinum-black coated platinum wire with 0.6 mm in diameter and 8.0 mm in length. A calibration curve shows good linearity and it is confirmed that the density of salt water is proportional to Cl^- concentration over the range of this measurement. The measurement of velocity was done with conical hot-film velocity meters. Since the output voltage of these probes is remarkably influenced by the variation of water temperature, the experiments had to be carried out under the same temperature in fresh water and salt water. Their output signals were recorded on a FM data recorder, and were played back to digitize to about 2400 data with 4-bits accuracy at an effective sampling frequency of 12.5 Hz.

Flow patterns at the water surface were observed by taking photographs of fluorescent dye or floats by means of a high-speed 16 mm cine-camera and a 35 mm camera.

The scheme of the experiments is given in Table 1. Independent variables are the jet velocity, U_o; the density deficit of the outfall water, $\Delta\rho_o = \rho_o - \rho_a$, where ρ_o is the discharge density at the outfall and ρ_a is the ambient density; the outfall width, B_o; and the outfall depth, H_o. They are grouped into the following dimensionless parameters.

Aspect ratio : $A = B_o / H_o$ (1)

Outfall Reynolds number : $Re_o = U_o H_o / \nu$ (2)

Outfall densimetric Froude number : $Fd_o = U_o / \sqrt{(\Delta\rho_o/\rho_a)\, g H_o}$ (3)

in which g = the acceleration of gravity and ν = the kinematic viscosity of discharged water.

Table 1 Schemes of experiments

Series	B_o(cm)	H_o(cm)	ε_o	Fd_o	Re_o
A	2.5	3.5	0.0 - 0.0165	1.74 - 14.36,	2510 - 10300
B	1.0	1.5	0.0 - 0.0150	0.72 - 4.10,	619 - 1239

Note : Series A for measurements and flow-visualization of particle paths, Series B for flow-visualization of streamlines, streaklines and particle paths.

Buoyant forces develop due both to (a) the density disparity between the discharge and the receiving water and (b) any density variation within the jet. Their effects bring out an elevation of water surface. Notwithstanding that the elevation and its gradient are too small to evaluate experimentally, they result in accelerating the lateral spread. Therefore, the relative density difference adds to dimensionless parameters.

Relative density difference : $\varepsilon_o = \Delta\rho_o / \rho_a$ (4)

Aspect ratio was fixed to a value of nearly 0.7 in both series of experiments, whose effect was not discussed.

HYDRAULIC CHARACTERISTICS AND ENTRAINMENT OF THREE-DIMENSIONAL BUOYANT SURFACE JET

In spite of many tests of the analytical models of surface buoyant jets on the basis of laboratory experiments and field observations, the hydraulic properties of entrainment remain unclear. The reason for insufficient understanding of this

process is that the experiments have been in the extension of the free turbulent jet and the buoyancy effects due to the density difference are treated only as additional terms. There is little information on the spread of three-dimensional buoyant surface discharges.

In this chapter, based on measurements of velocity and excess-concentration, the hydraulic characteristics are discussed and the entrainment hypothesis is applied to a three-dimensional problem.

Profiles of Velocity and Excess-concentration

Figure 1 shows a typical example of lateral and vertical profiles of time-mean velocity and excess-concentration, which were measured at cross-sections with various longitudinal distances. Their profiles are found to be geometrically similar. Especially, the relationship between U/U_s and y/B_e (and z/H_e) at the zone of established flow has the nearest similarity to the normal Gaussian curve regardless of Re_o and Fd_o. Functional expression are as follows :

$$U = U_s f(y/B_e) f(z/H_e) \quad ; \quad \Delta C = \Delta C_s g(y/B_e) g(z/H_e) \qquad (5)$$

in which $U_s(x)$ = surface velocity on the axis; $\Delta C_s(x)$ = surface excess-concentration on the jet axis beyond the concentration in ambient water; B_e and H_e = width and depth respectively at a fixed point where U/U_s is $1.0/e$ ($= 0.3679$); x = the longitudinal distance along the centerline of the jet measured from the point of

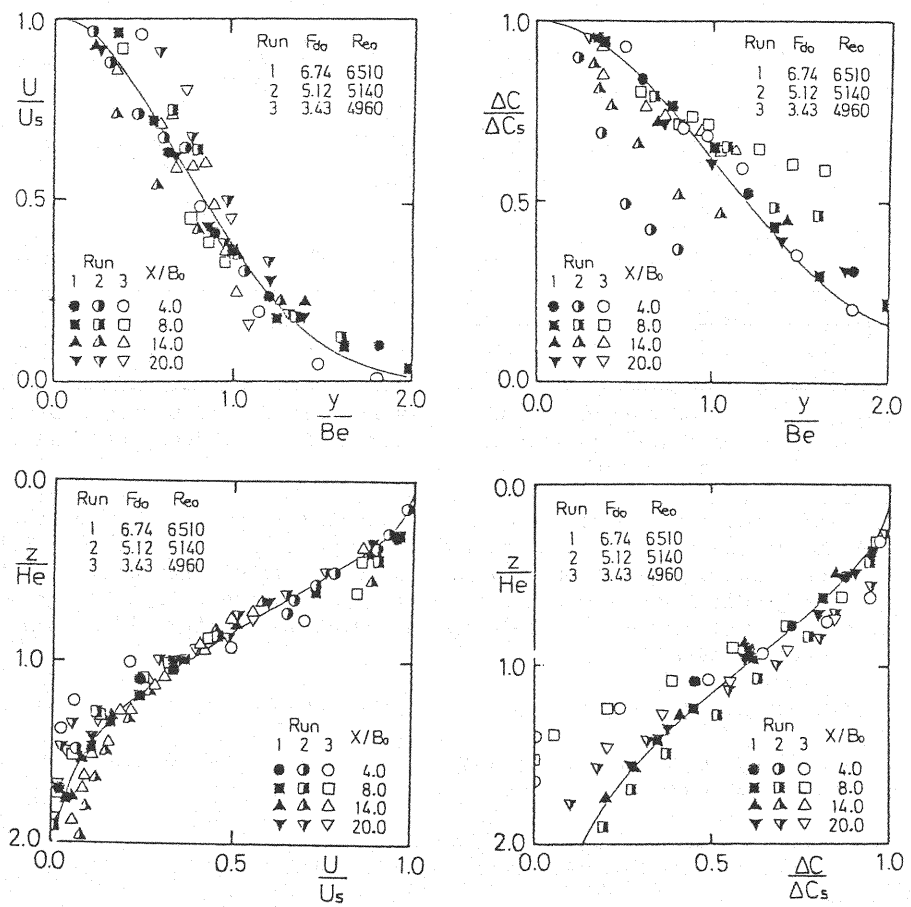

Fig. 1. Lateral and vertical profiles of time-mean velocity and excess-concentration

discharged outfall; y = the lateral distance measured normal to x; z = the vertical distance measured normal to x.

The similarity functions are the same as assumed by Hayashi, Miyahara and Arita (9), of which forms are given as follows :

$$f(t) = \exp(-t^2) \quad ; \qquad g(t) = \exp(-t^2/2) \tag{6}$$

When the cross-sectional profiles are established to be similar, the property of velocity reduction toward downstream is also expected to be adaptable to the case of buoyant surface jets on the basis of the conservation of momentum flux.

Figure 2 shows the distributions of dimensionless velocity and excess-concentration, U/U_o and $\Delta C/\Delta C_o$, along the jet axis measured at a depth of 1.0 cm beneath the water surface, in which U_o and ΔC_o are the velocity and excess-concentration at the outfall, respectively. Measured velocity curves are all drawn beyond the theoretical curve proposed by Albertson et al. (2) for fully submerged circular jet, which is indicated by a fine straight line in the same figure. The rate of decreasing is, however, still likely to obey the - 1st power of a distance from the outfall, x/B_o. This may have been caused by the slight difference of density, which must have affected the gravitational stability to restrain the surface buoyant jet from spreading in a vertical direction. At the same time the figure shows the fact that the rate of decreasing of U/U_o becomes smaller as the value of densimetric Froude number increases. The same trend is seen in the excess-concentration curves. In this case, however, the rate of decreasing is smaller and close to the - 1/2 power of x/B_o.

Figure 3 shows the relative intensities of the fluctuations of velocity u and concentration c along the jet axis. The relative intensities tend to rise rapidly from 30 % to 50 % toward the end of core region and to decrease gradually downstream. Considering that the time-mean velocity along the jet axis does not

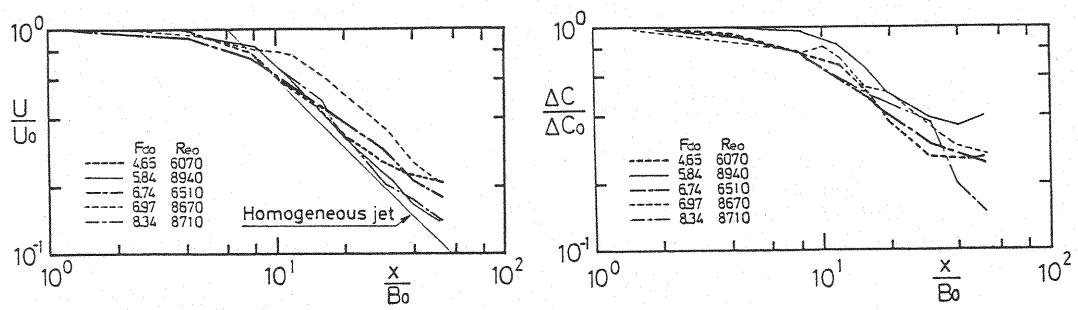

Fig. 2 Variation of time-mean velocity and excess-concentration along jet axis

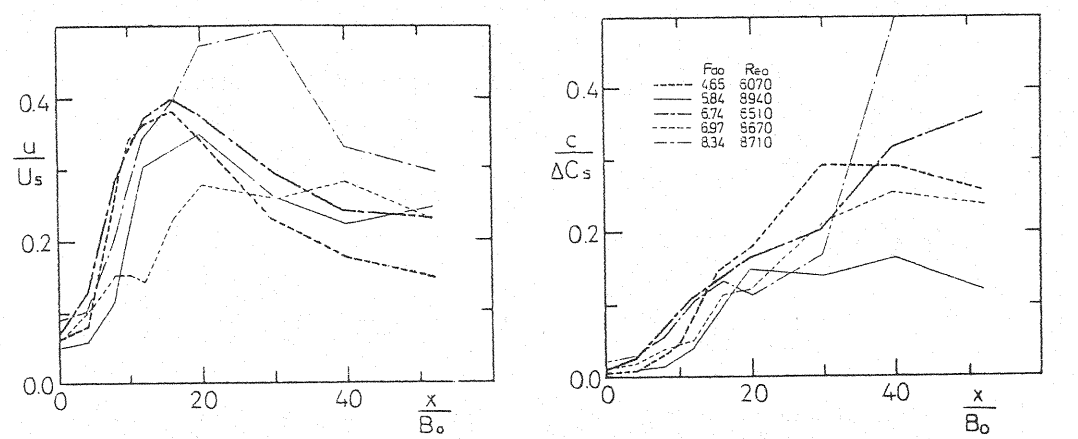

Fig. 3 Variation of fluctuating velocity and excess-concentration along jet axis

decrease with such a high rate, the rapid increase of the turbulent intensities must have been caused by the engulfing of ambient water outside the jet due to the initial momentum. It is proved that the maximum value of intensities increases in proportion to the densimetric Froude number, and, moreover, the location of peak intensities shifts downstream as the value of Reynolds number increases. The latter is in agreement with the corresponding experimental results of Dornhelm et al. (6), that is, the mixing of the jet occurs more strongly for the case of low Reynolds number. From the above facts, the interesting results may be concluded that although the time-mean profiles of the jet are self-preserving and are expressed as similar Gaussian curves regardless of hydraulic properties such as Fd_o and Re_o, the characteristics of fluctuating velocity are influenced significantly by them. On the other hand, the intensity of concentration fluctuation shows different characteristics, that is, it increases in the neighbourhood of the outfall and tends to continue to increase further in the downstream.

Spread of Buoyant Surface Jets

The lateral spreading widths are plotted in Fig. 4. B_n indicates the available width of a jet, because the line in the figure means the nominal boundary evaluated from the velocity profile at which the value of U/U_S is 0.02. B_{ap} is the width which is measured from a point at which the approaching velocity would be a minimum near the nominal jet boundary. The plotted points are considerably scattered, but it is clear that the lateral spread is influenced by the buoyancy. The spreading rate of the jet width, dB/dx lies in the range of 0.3 - 0.8 in the case of the buoyant surface jets, which is considerably larger than the value for a homogeneous jet, $dB/dx = 0.22$ proposed by Abramovich (1). In addition, its rate seems to increase in the case of larger densimetric Froude number.

On the other hand, Fig. 5 shows the distribution of the surface-layer depth H_R, the bottom of the layer being defined at a point where there is a sharp change in the local Richardson number Ri(z). Ri(z) is evaluated numerically from the formula :

$$Ri(z) = - (g\, dC/dz) / [C (dU/dz)^2] \qquad (7)$$

The depth at which the rapid increase in Ri occurs may be regarded as a stratified interface lying horizontally in the jet. With respect to the velocity and concentration fluctuations, the turbulence becomes weak and intermittent. Variations of H_e and the nominal boundary H_n are also plotted in the figure to compare with the velocity profiles.

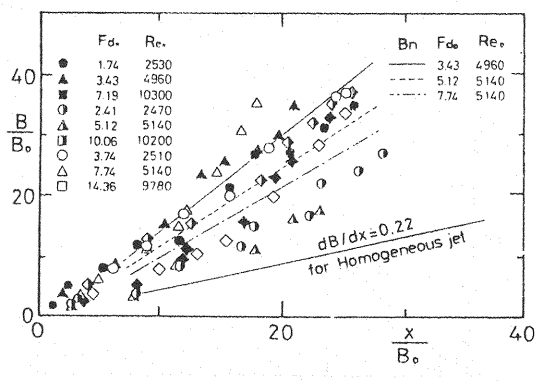

Fig. 4 Lateral spreading width for various Re_o and Fd_o

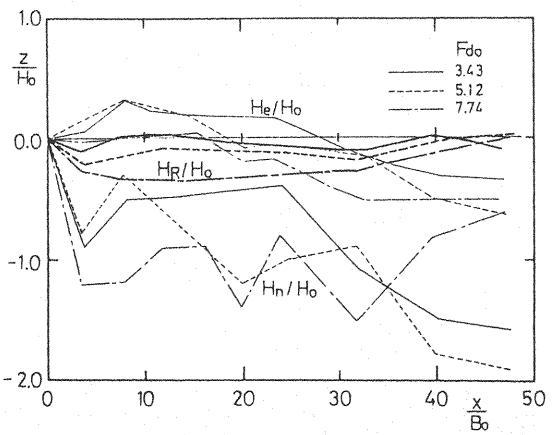

Fig. 5 Vertical spreading depth for various Fd_o

It is interesting to note that the variation of the depth dH_R/dx is extremely small, and no vertical spread is seen in the region of $x/B_o > 10$. The same tendency is observed in the velocity profiles indicated by H_e and H_n. Hayashi and Shuto (11) reported the same result based on temperature contours along the jet axis. Moreover, Murota and Nakatsuji (14) applied the conditional sampling and averaging analysis in order to make clear turbulence structure and obtained the result that the Brunt-Väisälä oscillation due to density difference was evidently predominant even at the interface at $x/B_o = 16$ of $Fd_o = 7.03$. That is, the vertical entrainment occurs only in the vicinity of the outfall. Thus, the buoyant surface discharge tends to retain its gravitational stability because of the slight difference in density, and this restrains the surface flow from spreading vertically while at the same time forcing the lateral extension. The magnitude of the density difference is represented by the densimetric Froude number, and in this sense it is possible to suggest that the densimetric Froude number may be an important parameter in connection with the vertical entrainment.

Evaluation of Vertical and Lateral Entrainment

Morton et al. (11) regarded entrainment as a phenomenon in which the ambient fluid is engulfed into the turbulent zone; this flow is directed perpendicular to the main flow direction and its velocity is proportional to that of the main flow. The constant of proportionality is called the *entrainment constant*. If the flow is in a state of local equilibrium, the entrainment constant is defined by local scales of length and velocity. Subsequently, Ellison and Turner introduced the overall Richardson number as an index of stability, that is, the ratio of the buoyancy to the inertia force. In this section, vertical and lateral entrained volumes are evaluated based on above-mentioned experimental results.

(a) Entrainment hypothesis

On estimating the entrained volume from ambient denser water, the longitudinal variation of mass flux integrated over the cross section is presented as follows :

$$\frac{dQ}{dx} = \frac{d}{dx}\int_0^{-\infty}\int_{\infty}^{-\infty} U\, dy\, dz = \oint_{\tilde{c}} \tilde{V}_E\, dc \qquad (8)$$

where $\tilde{V}_E$ denotes the entrainment velocity and $\tilde{c}$ the boundary of the jet mixing zone. As mentioned as to the experimental results, the buoyancy takes a dominant role in both entrainment process and lateral spread of the jet. Therefore, it is necessary to specify the velocity $\tilde{V}_E$ and turbulent transfer of heat and momentum.

In this analysis the structure of a surface buoyant jet is assumed as illustrated in Fig. 6. The velocity $\tilde{V}_E$ is separated into lateral and vertical components as follows :

$$\left.\begin{aligned} V_E / U_s &= \alpha_y = dB_A / dx \\ W_E / U_s &= \alpha_z = \beta \exp(C \overline{Ri}) \end{aligned}\right\} \qquad (9)$$

where α_y and α_z are entrainment coefficients in lateral and vertical directions.

Although Eq. 9 does not satisfy exactly the lateral momentum equation, such an assumption is introduced as a matter of convenience from the analogy of a homogeneous jet. α_y is to be determined with relation to the longitudinal variation of the width, B_A. B_A is a newly-defined width where an accumulated area is half of the area of velocity profile. On the other hand, α_z is postulated in the exponential form based on Ellison and Turner's experiment (7). Their data demonstrates that the vertical entrainment velocity, W_E, is a function of the overall Richardson number, $Ri = \varepsilon g H / U_s^2$, in two-dimensional buoyant jet and that the values β and C are 0.075 and 5.0 respectively.

In three-dimensional buoyant jets, it becomes a serious matter of great concern how the vertical entrainment is estimated in connection with lateral spread due to buoyant effect. Considering the similarity functions and the width of the jet in integration of Eq. 8, the entrainment volume, Q_E, is given by the summation

of vertical and lateral ones by the following expression :

$$Q_E = Q_z + Q_y = 2\,\alpha_z(0)\,U_s\,B_e\,I + 2\,\alpha_y(0)\,U_s\,H_e\,I \qquad (10)$$

where

$$I = \int_0^\infty \exp(-t^2)\,dt.$$

The above equation has contradictory content that the vertical entrainment increases conversely as the stratification grows and promotes the lateral spread. It is because that Q_z increases in proportion to the width B_n of the jet. Then, assuming that the vertical entrainment coefficient $\alpha_z(y)$ should vary corresponding to the change of the overall Richardson number $\overline{Ri}(y)$ in lateral direction, the reduction of $\alpha_z(y)$ is introduced in the next modified form :

$$\frac{\overline{Ri}(y)}{\overline{Ri}(0)} = \exp\left[\frac{3}{2}\left(\frac{y}{B_e}\right)^2\right]\sqrt{1-\left(\frac{y}{B_e}\right)^2} \qquad (11)$$

Figure 7 shows the lateral variation of the overall Richardson number, $\overline{Ri}(y)$. As shown in this figure, its value increases quite rapidly with the increase of y/B_e. According to Ellison and Turner's results, the vertical entrainment vanishes in the range where the value of $\overline{Ri}$ exceeds 0.85. The range corresponds to $y/B_e > 1.0$, when $\overline{Ri}(0)$ is chosen to be 0.2 in this case. Then, if the entrainment constant α_z is calculated using Eqs. 9 and 11, $\alpha_z(y)/\alpha_z(0)$ indicated by the plots in the same figure tends to decrease in the region laterally far from the jet axis. The above consideration suggests that the estimation of vertical entrainment should be corrected as follows :

$$Q_z = \int_{-\infty}^{\infty} W_E\,dy = 2\int_0^\infty \alpha_z(y)\,U_s \exp\left[-\left(\frac{y}{B_e}\right)^2\right] dy \qquad (12)$$

where

$$\alpha_z(y) = \beta \exp\left[-C\,\overline{Ri}(0)\exp\left\{\frac{3}{2}\left(\frac{y}{B_e}\right)^2\right\}\sqrt{1-\left(\frac{y}{B_e}\right)^2}\,\right].$$

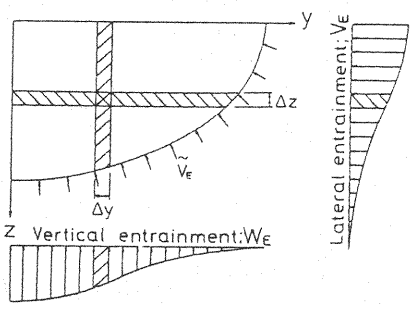

Fig. 6 Schematic of entrainment velocity

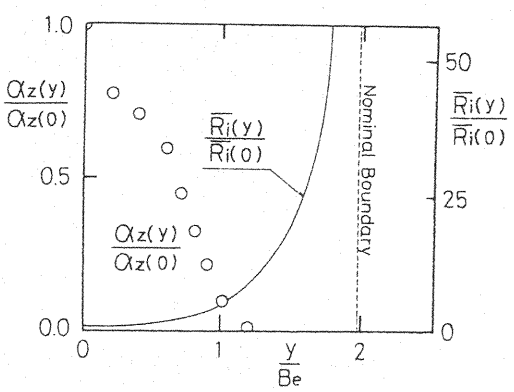

Fig. 7 Relation between vertical entrainment constant and overall Richardson number

(b) Comparison between predicted results and experimental data

In this article the adequacy of the entrainment hypothesis is discussed in the zone of established flow, $x/B_o > 8$, in which the similarity functions are applied. Figure 8 shows the variation of the integrated volume $Q(x)$ along the jet axis. The predicted volume indicated by the straight lines are calculated in the matter of added entrainment volume $Q_z + Q_y$ against the measured volume at the point of $x/B_o = 8$ step by step. At that point, it is assumed that the mixing caused by the initial momentum transfer of the jet is finished, and the integrated volume appears

to be sensitive to the value of Fd_o. On the other hand, the values of volume obtained from the measured velocity profiles are plotted in the figure.

As shown in Fig. 8, it is recognized that the predicted results agree reasonably with the experimental results for $8 < x/B_o < 40$ and the density effect is well reflected upon these results. To say conclusively, the entrainment hypothesis proposed here could satisfactorily explain the spread of three-dimensional buoyant surface jets. In Fig. 8, the increasing rate of the integrated volume decreases gradually in the region of $x/B_o > 32$, as contradicted with Albertson's theoretical curve showing a uniform increase in the region far from the origin of the jet.

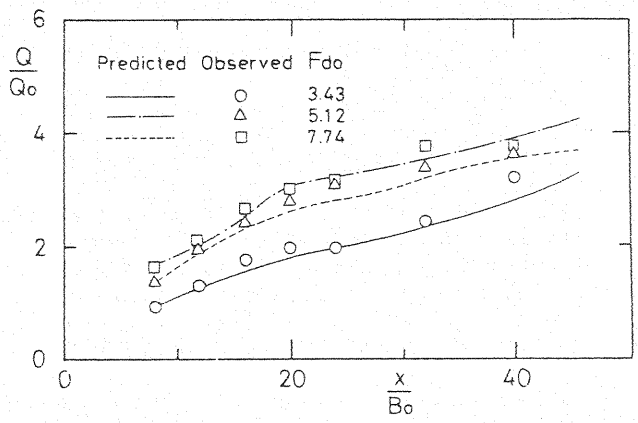

Fig. 8 Comparison between estimated volume and experimental data

Figure 9 illustrates the ratio of lateral entrained volume and vertical one, Q_y/Q_z. It shows a very interesting tendency that the value of Q_y/Q_z decreases and reaches minimum in the range of $12 < x/B_o < 16$, and beyond that point it increases monotonously. This fact shows that the vertical entrainment is restricted in the zone of established flow, and the lateral spread due to stratification makes the lateral entrainment large quantitatively compared with the vertical one. Thus, a buoyant surface jet has a special mixing process at a part not so far from the jet outfall even in the zone of established flow, but becomes similar to that of two-dimensional plane jet in the part for $x/B_o > 30$ or 40.

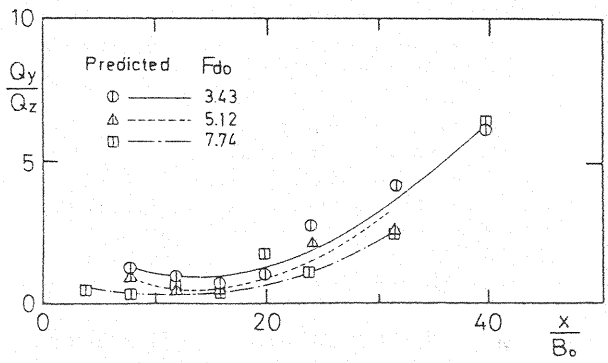

Fig. 9 Variation of ratio of lateral entrained volume and vertical entrained one, Q_y/Q_z along jet axis

VISUALIZATION OF SURFACE FLOW PATTERN

In this chapter the mechanism of lateral gravitational spread in the near field is clarified by means of flow-visualization technique in relation to outfall hydraulic characteristics such as densimetric Froude number, Reynolds number and relative density difference.

Quantitative analysis was carried out, based on the information of surface flow patterns at the outside of a jet, because the motion of fluid particles contains integrated information associated with the vortex evolution and the entrainment process. Another reason to use this procedure is that an accuracy in a velocity measurement is still satisfactory because the fluid motion is non-irrotational and non-turbulent.

In order to visualize the flow pattern at the water surface, small solid particles or dye are released into the fluid. This foreign material is moved along with the mean flow. The motion and trace of this material can be measured by means of some visualization techniques :

a) Streamlines can be photographed with an appropriate and known exposure time by

means of a 35 mm still-camera, which enable to obtain the magnitude and direction of velocity. Aluminum powder was used as a tracer and cleanser was dissolved in water at the rate of 75 g per 1000 liter for diminishing surface tension.

b) Streaklines are the instantaneous loci of all particles. They could be visualized by continuously injecting dye buoyant-neutrally controlled by Rohdamine-B and alcohol into the flow from the vicinity of the outfall. A high-speed 16 mm cine-camera was used.

c) Particle paths contain the integrated time history of the motion of one single particle. It can be visualized if one takes a long-time exposure photograph of the motion of a small particle, or if one takes a locus of the particle as a function of time. A 35 mm still-camera or a 16 mm cine-camera was used.

Vortex Evolution at the Zone of Flow Establishment

High-speed motion-picture films were taken to investigate the evolutionary phenomena of initial instability at the water surface. Figure 10 illustrates behaviors of dye streaks from two dye-injectors located at both sides of the outfall. This example is a case of Re_o = 867 and Fd_o = 1.94. Flow is from left to right. The time increment between successive illustrations is 0.25 second. Dye streaks, straightly flowed at an initial stage, become unstable and concentrated into small disturbances at points A, B and C as shown in the figure. These small disturbances occasionally break up and form vortex-like structures. At three or four wavelength apart from the outfall, they are observed to disperse across the entire width of a jet. This instability is affected considerably by the outfall Reynolds number and the density difference. That is, the instability becomes evident with increasing Reynolds number, and neighbouring pairs of vortical structures are often seen to roll around each other to amalgamate into a larger one. In the case of larger density difference, the instability point goes away from the outfall and disturbances have a tendency not to amplify in the flow direction.

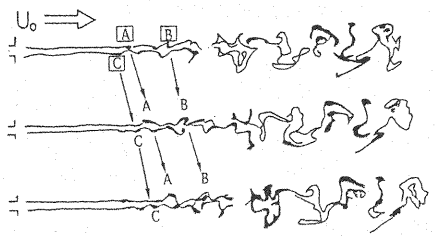

Fig. 10 Schematic of streaklines illustrating vortex evolution

Quantitative data for the initial instability can be reduced from high-speed films which were taken at the rate of 24 flames per second. They are the dimensionless length, L_o/B_o from the outfall to the point where dye streaks become unstable or roll back, and the dimensionless frequency, f_oB_o/U_o (= St_o; Strouhal number), in which f_o represents the occuring frequency of instability. They are shown in Fig. 11 and Fig. 12 respectively. L_o is the length of the potential core, that is, the length of the zone of flow establishment. The general trend of L_o/B_o is to vary inversely as the square root of the Reynolds number : $L_o/B_o = a_1/\sqrt{Re_o}$. The same trend has been observed in several other investigations, for example

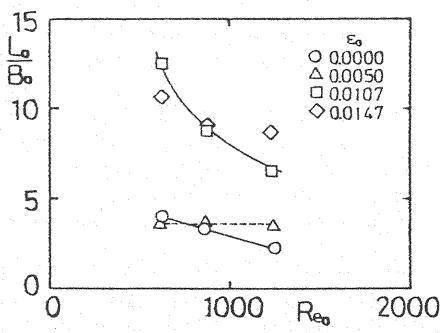

Fig. 11 Length scale of initial instability

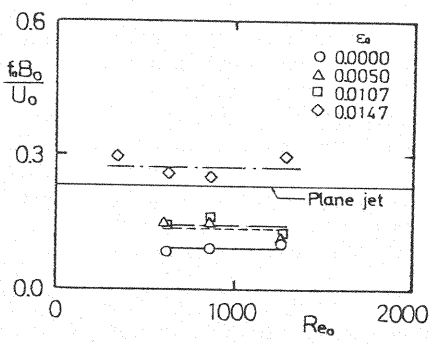

Fig. 12 Strouhal number of initial instability

Becker and Massaro (5). The constant value, a_1 is different according to a relative density difference. Figure 11 indicates that the potential core shortens with increasing Re_o and ε_o.

On the other hand, each value of Strouhal number for various density difference is almost equal independent of the Reynolds number. Its value tends to increase with increasing density difference. In the case of $\varepsilon_o = 0.0147$, the Strouhal number is found to remain constant at $St_o = 0.28$. This value is relatively close to the value of $St_o = 0.23$ obtained by Sato (17) for a two-dimensional jet for the range of Reynolds number from 1500 to 8000. Beaver and Willson (4) examined $St_o = 0.43$ of plane jets issuing from sharp edged slit within a range of $500 \leq Re_o \leq 3000$. Comparison of the value of this experiment to published data indicates that a buoyant surface jet behaves just like a horizontal plane jet in larger density differences.

Streamlines and Particle Paths at the Boundary and the Outside of a Jet

The set of photographs shown in Figs. 13 and 14 shows a typical example of spreading patterns of homogeneous and buoyant surface jets. Figure 13 was taken at an exposure time of 0.5 second. Therefore, it represents streamlines drawing the field of velocity vectors in the boundary and the outside of a jet, while it does particle paths in the high-speed inside. Figure 14 shows long-time exposure photographs of fluorescent styloform particles in a dark room. The particle paths during 15 seconds are visualized to illustrate the motion of single particles entrained into the jet. A close inspection of the photographs reveals the following features :

a) In homogeneous surface jets, fluid particles near the outfall ($x/B_o < 20$) converge into the vicinity of $x/B_o = 10$ and entrained into the jet. This phenomenon is intimately related to the vortex shedding in the free shear layer as described concerning streaklines. The jet discharge begins meandering slightly around the main trajectory owing to the vortex evolution.

b) In the downstream region where $x/B_o > 20$, large scale turbulent vortical lumps are apparently visualized along the jet boundary over a wide range of $x/B_o = 10 \sim 40$, and they take place symmetrically in regard to the jet axis. The vortical lumps have a tendency to rotate in the outward direction from the jet axis. The inward streamlines are dense at the upper stream side, while the outward ones are sparse at the lower stream side. This implies that irrotational fluid at the outside of jets is engulfed into the jets at a faster speed at the upper stream side of the vortical lumps, and that a turbulent interface is moved outward at the lower stream side. In some cases a pairing between adjacent lumps is observed. This process is very similar to the development of turbulent shear layers and is essential in the lateral spread of homogeneous surface jets. Then, particle paths go around the boundary and move inward due to the vortical motion as shown in Fig. 14(a). Brightness observed at paths indicates the

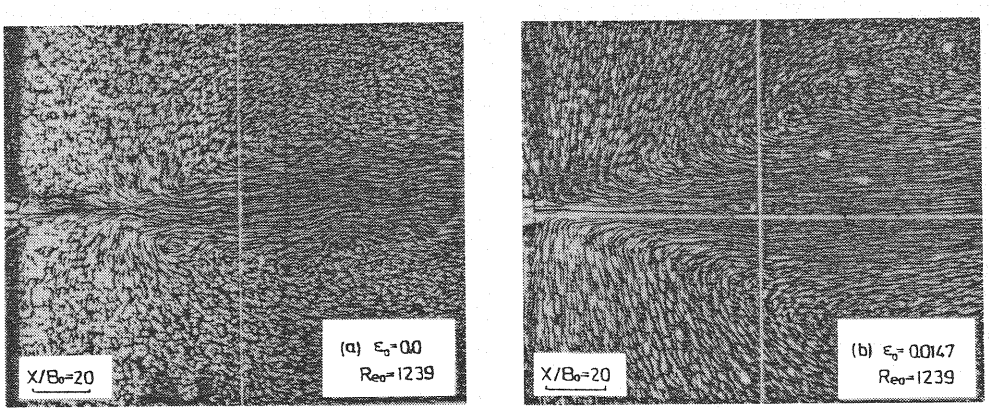

Fig. 13 Streamlines along jet boundary

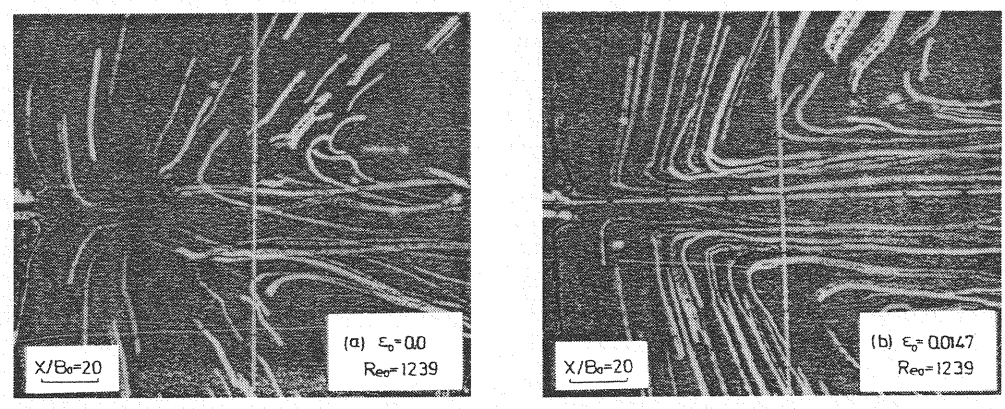

Fig. 14 Particle patns at the water surface

magnitude of a convective velocity. A rotating path observed at x/B_o = 35 is reflected in the vortical motion shown in Fig. 13(a). It is conjectured from this fact that the movement at the outside of the jet is caused by the vortical lumps developed at the jet boundary.

c) In buoyant surface jets in which the densimetric Froude numbers are less than 4.0, lateral entrainment takes place in the vicinity of the outfall. It is scarcely possible to observe vortical lumps at the jet boundary at an exposure time of 0.5 second. The pattern of streamlines shown in Fig. 13(b) is quite different from that of homogeneous ones shown in Fig. 13(a). Increased buoyancy of the discharge seems to suppress the vortex formation. Therefore, although the particle paths near the outfall are observed to approach at right angles to a jet axis, paths go around along the boundary owing to the vortical motion in the far region where buoyancy effects gradually decrease. As shown in Fig. 14 (b), particle paths are much longer as compared with that in Fig. 14(a). This result indicates that an approaching velocity is accelerated by buoyancy effects. Another feature of buoyant surface jets is that entrained fluid particles do not reach the center line of a jet.

d) Spread of the width of buoyant surface jets is fairly wider compared with that obtained in homogeneous jets, and is also wider than a velocity half width determined from the velocity profiles. It is more apparent for large density difference, in other words for small densimetric Froude numbers.

The possibility whether vortical lumps exist or not is examined from the photographs as shown in Fig. 13 as an example. The result is shown in Fig. 15, in which an exposure time of 0.5 second is used. Even in buoyant surface jets, the existence of visible vortical lumps is recognized with an increase of the Reynolds number or with a decrease of the density difference. The dependence on the densimetric Froude number appears to be much stronger than other parameters such as Re_o and ε_o.

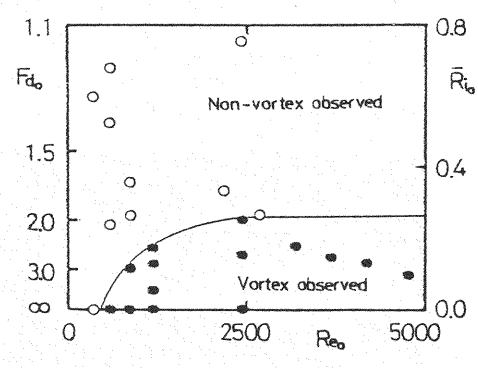

Fig. 15 Observation of vortical structures along jet boundary

Discussions

In order to provide useful information for constructing mathematical models of buoyant surface jets taking account of buoyancy effects, quantitative data must be reduced from the surface flow patterns in the outside of jets.

(a) Initial entrainment

Figure 16 shows a dimensionless length, L_E/B_o as a function of the outfall Reynolds number and the density difference, which can be determined as a distance, L_E from the outfall to the point where fluid at the water surface starts to be entrained into jets. Data of homogeneous plane jets are also plotted in the figure. Note that L_E is equivalent to the length of the zone of flow establishment in homogeneous surface and plane jets and that its length grows shorter with increasing Reynolds number. On the other hand, L_E/B_o in buoyant ones is as short as about 1.0 regardless of the value of ε_o and Re_o. Their trend is quite different with the length L_o/B_o obtained from the streaklines, which is closely related to the vortex evolution. In attempting to explain this apparent discrepancy, one must consider the buoyancy effects upon entrainment.

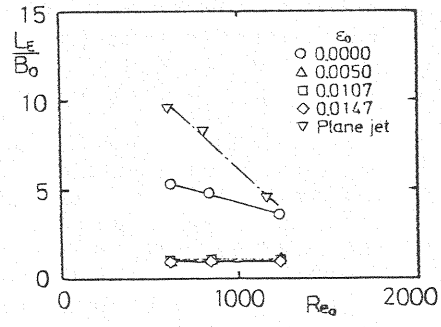

Fig. 16 Beginning point of entrainment

Next, in order to illustrate characteristic features concerning initial entrainment, the variation of an approaching velocity, V_{ap}/U_o and an angle, θ between the direction of particle paths and the jet axis with distance from the outfall are examined. V_{ap} is calculated from measuring a displacement of particles moved during 15 seconds. Figure 17 shows V_{ap}/U_o and θ in the case of Re_o = 619, 1239 and ε_o = 0.0, 0.0147. As an average, V_{ap}/U_o in a buoyant surface jet of ε_o = 0.0147 is three times higher than that in a homogeneous jet, and it tends to decrease gradually with downstream distance. The effect of Reynolds number seems to be much stronger in buoyant jets. In homogeneous surface jets, however, V_{ap}/U_o seems to be independent of the Reynolds number.

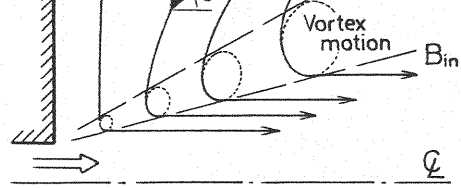

Fig. 18 Schematic illustrating particle paths

A general trend of θ is close upon 90° with an increase of Reynolds number. It suggests that fluid particles seem to approach falling at the right angles with a jet axis. And the gradual decreasing of θ with distance is generally found. Its tendency is more apparent for homogeneous jets. It reflects in the particle paths such that particles in the outer region approach boundaries making an angle less than 90° and are entrained into the jet due to the vortical motion as shown in Fig. 18.

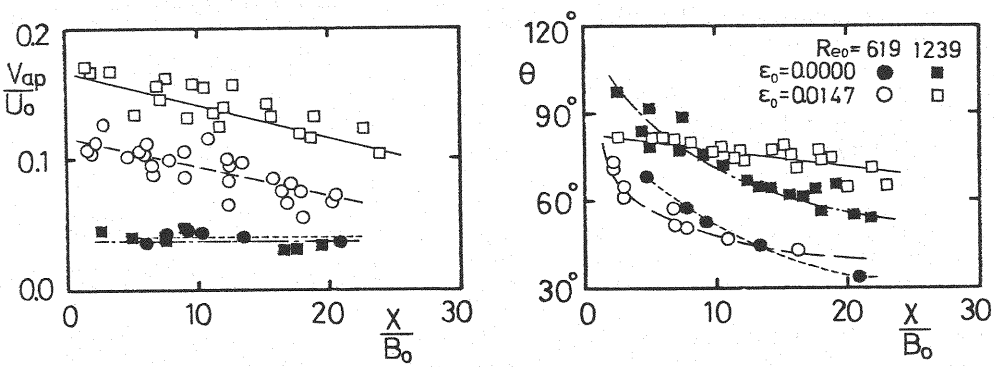

Fig. 17 Variation of approaching velocity and its angle with distance

Another characteristic velocity is a lateral component of V_{ap} meeting at a right angle with the jet axis, represented by $\hat{V}_E$. The dimensionless velocity $\hat{V}_E/U_s$ is a lateral entrainment coefficient, α_E defined by Morton et al., in which U_s is a longitudinal velocity at the centerline of jet at the water surface. The variation of α_E with distance is as follows, although it is not illustrated.

a) In buoyant surface jets the value of α_E is more significant in the zone of flow establishment with increasing density difference.
b) There is a gradual decrease of α_E to reach a minimum value near the point x/B_o = 6.0. Beyond this point α_E increases again to almost constant value of 0.11 ~ 0.13 in the zone of established flow.
c) On the other hand, α_E in homogeneous surface jets increases monotonously from the entrainment point $x = L_E$ and becomes 0.075 ~ 0.08 at the zone of established flow. Its value is lower than that obtained in buoyant surface jets.

(b) Effects of the Reynolds number on entrainment pattern

From an empirical viewpoint, it may be stated that the velocity profile in a buoyant jet is not substantially affected by the Reynolds number as long as the flow is turbulent. Nevertheless, it remains to ask whether the Reynolds number plays a significant role in the entrainment process in spite of turbulent phenomena. In observations of particle paths on the water surface as shown in Fig. 19, it is found that the flow patterns may be grouped in three different categories according to the magnitude of the Reynolds number.

Type I is the irrotational flow pattern, in which particles circulate slowly along the boundary in the opposite direction to the jet flow and are finally engulfed by the jet. In this case, $Re_o \simeq 2800$. With increase in Reynolds number, this pattern is replaced by the transitional type II in which particles approach close to the jet axis and move downstream, rotating slightly near the jet boundary, and are then engulfed into the jet. Lastly, in Type III with $Re_o > 11000$, particles also approach close to the jet axis and are entrained as they are whirling.

Thus it seems that the Reynolds number is directly related to the development of the jet boundary or the vortical motion in that layer, and plays an important role in characterizing the entrainment process, although it has little effect on the mean values of hydraulic quantities inside the buoyant jet.

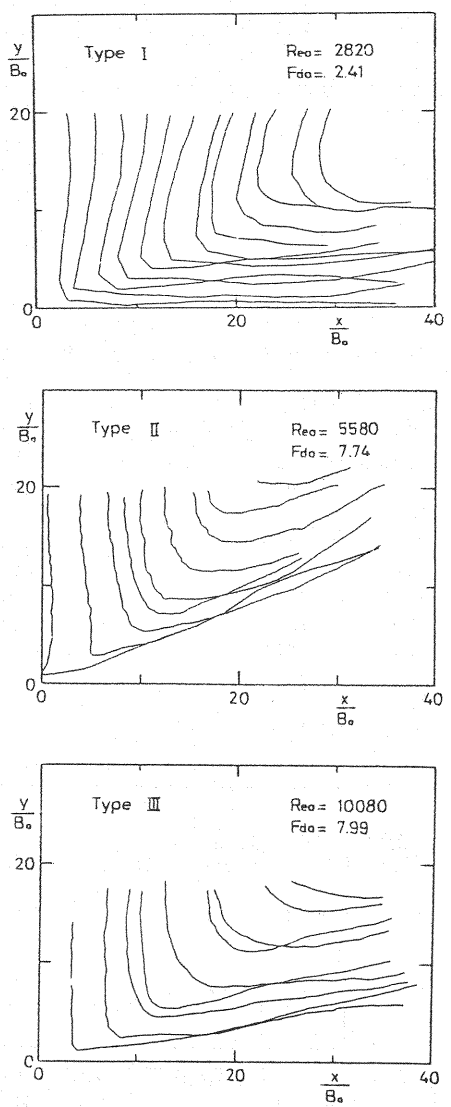

Fig. 19 Particle paths with various Re_o and Fd_o

(c) Spread of jet widths

Figure 20 shows jet widths as a function of the distance from the outfall to distinguish spread caused by buoyancy effects and the vortical motion. The outer and inner boundaries, represented by B_{out} and B_{in} respectively, are newly defined based on the paths of floating particles, that is schematically shown in Fig. 18. Each line in Fig. 20 is an average of four to five instantaneous pictures. It is of some interest in homogeneous jets to note that a velocity half width and a nominal boundary correspond markedly well to the inner

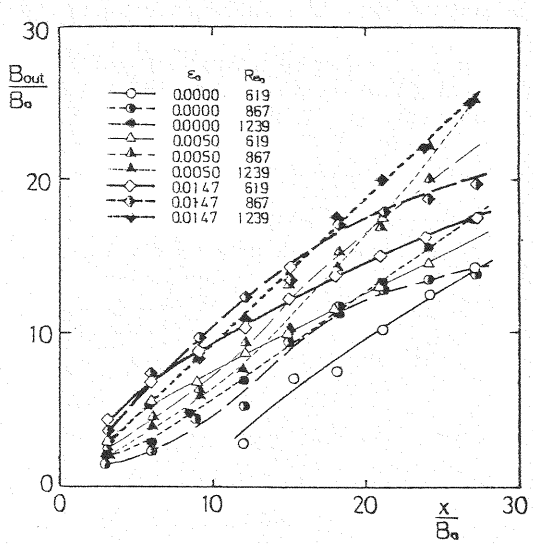

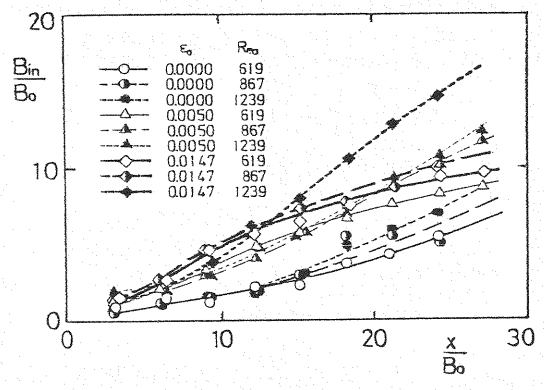

Fig. 20 Jet width as a function of the distance

and the outer boundaries respectively, which is ascertained by Muraoka and Nakatsuji (14).

With respect to the inner boundary, it is apparent that an increase in density difference results in widening of jet widths especially in the zone of flow establishment. The variations with Reynolds number are found slightly in the zone of established flow. The effect of Reynolds number is more subtle than the effect of density difference. On the other hand, spread of the outer boundary increases with increasing density difference, in which the effect of Reynolds number can be seen clearly. It is worthy to note that B_{out}/B_o in the case of Re_o = 619 and ε_o = 0.0 is extremely small because of imperfect development of vortical structures and that B_{out}/B_o in the case of Re_o = 1239 is smaller than that of the lower Reynolds number in buoyant surface jets. It can therefore be expected that the buoyancy effect in the outer boundary fades out with increasing Reynolds number and that the vortical motion exerts influence upon the entrainment process.

Then, to examine correlations of the approaching velocity and the densimetric Froude number with the spreading rate of the jet width, Figs. 21 and 22 are prepared. In Fig. 21, a linear relationship between V_{ap}/U_o and dB_{in}/dx can be seen provided that the mean values within a range of $x/B_o < 12$ are used. This means that the increase in lateral spread due to the buoyancy is intimately related with

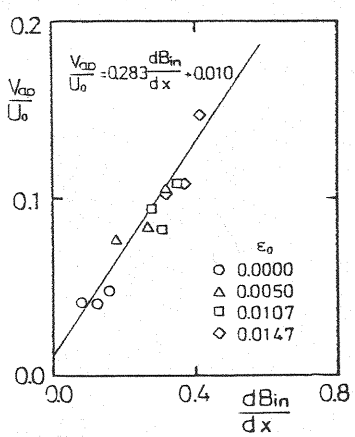

Fig. 21 Relation between approaching velocity and lateral spreading rate

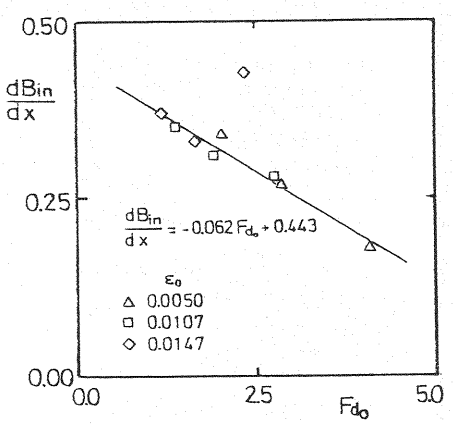

Fig. 22 Relation between lateral spreading rate and densimetric Froude number

initial entrainment immediately. It might be argued that the buoyancy counteracts the vertical entrainment and thereby increases the lateral entrainment through lateral spread. Furthermore, an intimate relation between dB_{in}/dx and Fd_o is also recognized. That is shown in Fig. 22. From these figures, the following relationship for the approaching velocity in the zone of flow establishment can be derived:

$$Vap/Uo = -0.018\,Fd_o + 0.135 \qquad \text{for} \quad Fd_o < 5.0. \tag{13}$$

A simple model for spread of buoyant discharges floating at deep water is formulated by considering density induced motion by Weil and Fischer (23) and Koh (12). Assuming that lateral front motion of buoyant discharges is caused by the front velocity of an idealized rectangular layer, the convective velocity is expressed as

$$u_f = c_1 \sqrt{\varepsilon g h} \tag{14}$$

in which c_1 = a constant coefficient which depends on front conditions; h = a layer depth; and 2b = a layer width.

The layer is spread in the lateral direction by the front velocity, u_f, and at the same time moved downstream by the longitudinal velocity, u_x ;

$$u_f = db/dt \quad ; \quad u_x = dx/dt \tag{15}$$

When Eqs. 14 and 15 are combined, an expression for the layer width becomes

$$\sqrt{b}\, db = \frac{1}{\sqrt{2}}\, c_2 \sqrt{\varepsilon g a}\, \sqrt{a}\, \frac{1}{u_x}\, dx \tag{16}$$

in which $a^2 = 2bh$.

Provided that mixing does not occur within the layer and that the longitudinal convection velocity does not change, that is, ε and u_x are constant with distance, an integration of Eq. 16 leads to a simple form.

$$\frac{b}{\sqrt{B_o H_o}} = c_2\, Fd^{-2/3} \left(\frac{x}{\sqrt{B_o H_o}} \right)^{2/3} \tag{17}$$

The width, b in Eq. 17 is a spreading width due to buoyancy alone. Therefore, to verify the validity of Eq. 17, it is required to use the following relation that the width is defined as the width of buoyant surface jets minus the width of homogeneous ones such that $b = \Delta B = B_{in} - [\, B_{in} \,]_{\varepsilon = 0.0}$.

In Fig. 23 this relation is compared with experimental data. The agreement is acceptable for data obtained near the outfall and data of $Fd_o < 2.3$, in which Fd_o at the outfall is adopted instead of Fd(x). The disagreement observed in the far region from the outfall is probably due to the above-mentioned assumptions introduced in the derivation of Eq. 17. Of course, the variation of Fd with the distance from the outfall must also be taken into account. The results presented so far are encouraging except for discrepancies in the zone of established flow. It is possible to be improved by considering the variation of density deficit and densimetric Froude number.

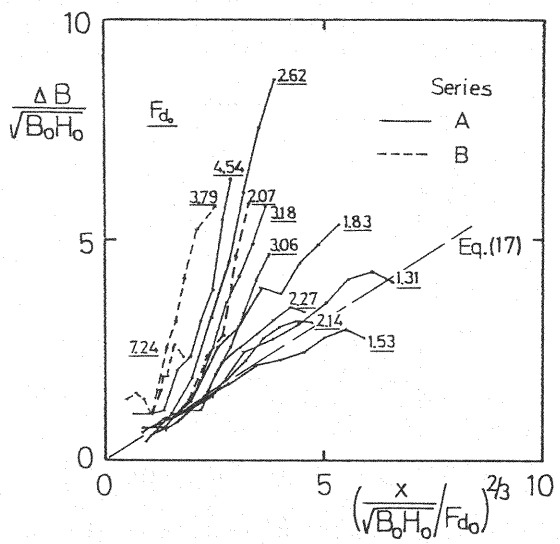

Fig. 23 Spread of widths due to buoyancy alone

CONCLUSION

A realistic picture of the flow field of three-dimensional buoyant surface jets with rather small densimetric Froude numbers can be drawn on the basis of measurements of velocity and excess-concentration and flow-visualization of the surface flow patterns. The following conclusions can be made :

(1) The growth and decay of vortical structures at the jet boundary have direct effects upon the engulfing of ambient fluid. Reynolds number is so related only to the behaviors of vortical structures and the fluctuating properties of velocity and excess-concentration, but not related to their time-mean profiles, which are represented by similarity functions respectively.

(2) In buoyant surface jets, the slight difference of density accelerates the gravitational stability. Its property is to restrain the jets from vertical entrainment and to encourage them to spread in a lateral direction. It is confirmed by the variation of the ratio of lateral entrained volume and vertical one with the distance from the outfall, which are evaluated by means of the proposed method using the entrainment hypothesis.

(3) In the case of larger density difference, the vortex evolution at the zone of flow establishment is quite alike that in a horizontal plane jet.

(4) Spread of the width of buoyant surface jets is fairly wider compared with that obtained in homogeneous surface jets, and is also wider than a velocity half width determined from the velocity profile. Lateral spread is caused by both the stratification due to the density difference and the vortical motion developed at the jet boundary. In the vicinity of the outfall, the former factor becomes predominant because of much density disparity between the discharge and the receiving water. Therefore, the intense lateral entrainment takes place even near the outfall and its velocity is markedly high.

(5) Lateral spread due to buoyancy alone can be explained in terms of the density-induced front motion of buoyant discharges.

ACKNOWLEDGEMENT

The experiments and data processing were performed with the cooperation of Mr. Masahiro Kurimoto at Okumura-Gumi Co., and Mr. Yasuo Hozaki at Japan Highway Public Corporation, when they were graduate students at Osaka University. The authors gratefully acknowledge the help given by them.

REFERENCES

1. Abramovich, G.N. : The Theory of Turbulent Jets, MIT Press, Cambridge, Mass., pp.663, 1963.
2. Albertson, M.L., Y.B. Dai, R.A. Jensen and H. Rouse : Diffusion of submerged jets, Trans. ASCE, Vol.115, pp.639-677, 1950.
3. Asaeda, T. and N. Tamai : Turbulent entrainment in stratified flows, Proc. 3rd Int. Symp. on Stochastic Hydraulics, Tokyo, Japan, pp.445-456, 1980.
4. Beavers, G.S. and T.A. Wilson : Vortex growth in jets, J. Fluid Mech., Vol.44, Part 1, pp.97-112, 1970.
5. Becker, H.A. and T.A. Massaro : Vortex evolution in a round jet, J. Fluid Mech., Vol.31, Part 3, pp.435-448, 1968.
6. Dolnhelm, R., M. Nouel and R.L. Wiegel : Velocity and temperature in buoyant surface jet, Proc. ASCE, Vol.98, No.P01, pp.29-47, 1972.
7. Dunn, W.E., A.J. Policastro and R.A. Paddock : Surface thermal plumes : Evaluation of mathematical models for the near and complete field, Argonne National Lab., ANL/WR-75-3, Part 1 and 2, 1975.
8. Ellison, T.H. and J.S. Turner : Turbulent entrainment in stratified flows, J. Fluid Mech., Vol.6, pp.423-448, 1959.
9. Hayashi, T., H. Miyahara and M. Arita : A mathematical model on the spread of heated water discharged horizontally at the water surface, U.S.-Japan Seminar " Engineering and environmental aspects of waste heat disposal ", Tokyo, Japan, 1974.

10. Hayashi, T. and N. Shuto : Diffusion of warm water jets discharged horizontal -ly at the water surface, Proc. 12th IAHR Congr. Vol.4, pp.47-59, 1967.
11. Hayashi, T. and A. Shuto : Basic experiment on heated water jet discharged at water surface, Proc. of the 23th Japanese Conference on Hydraulics, JSCE, pp. 405-414, 1979. (in Japanese)
12. Koh, R.C.Y. : Buoyancy-driven gravitational spreading, Proc. 15th Coastal Eng. Confer., pp.2956-2975, 1976.
13. Morton, B.R., G.I. Taylor and J.S. Turner : Turbulent gravitational convection from maintained and instantaneous sources, Proc. Roy. Soc., Rondon A, Vol.234, pp.1-23, 1956.
14. Muraoka, K. and K. Nakatsuji : Entrainment constants in three-dimensional surface buoyant jet, Technol. Repts. Osaka Univ., Vol.27, No.1389, pp.537-545, 1977.
15. Muraoka, K. and K. Nakatsuji : Recent advances in hydrodynamic treatment for a buoyant surface discharge, Advances in Environmental Science and Eng., Vol.3, pp.30-55, 1979.
16. Murota, A. and K. Nakatsuji : Coherent structure and water quality transfer at stratified interface of buoyant surface jet, Proc. 3rd Int. Symp. on Stochastic Hydraulics, Tokyo, Japan, pp.643-654, 1980.
17. Sato, H. : The stability and transition of a two-dimensional jet, J. Fluid Mech., Vol.7, pp.53-80, 1960.
18. Stefan, H., L. Bergstedt and E. Mrosla : Flow establishment and initial entrainment of heated water surface jets, St. Anthony Falls Hydr. Lab., Univ. of Minnesota, EPA-660/3-75-014, 1975.
19. Stefan, H. and P. Vaidyaraman : Jet type model for the three-dimensional thermal plume in a cross-current and under wind, Water Resour. Res., Vol.8, No.4, pp. 998-1014, 1972.
20. Stolzenbach, K.D. and D.R.F. Harleman : An analytical and experimental investigation of surface discharges of heated water, Ralph M. Parsons Lab. for Water Resources and Hydrodyn., MIT Rep. No.135, 1971.
21. Tamai, N. : Surface discharge of horizontal buoyant jets, Coastal Eng. in Japan, Vol.12, JSCE, pp.159-177, 1969.
22. Tamai, N., R.L. Wiegel and G.F. Tornberg : Horizontal surface discharge of warm water jets, Proc. ASCE, Vol.95, No.PO2, pp.253-276, 1969.
23. Weil, J. and H.B. Fischer : Effect of stream turbulence on heater water plumes, Proc. ASCE, Vol.100, No.HY7, pp.951-970, 1974.

APPENDIX - NOTATION

The following symbols are used in this paper :

a	= layer depth of buoyant discharge;
A	= aspect ratio;
b	= half layer width of buoyant discharge;
B_o	= width at the outfall;
$B_{\hat{e}}$, $B_{\hat{n}}$, B_A, B_{in}, B_{out}	= jet widths;
c_0, c_1, c_2	= constants;
$\tilde{c}$	= boundary of jet mixing region;
c'	= rms value of fluctuating excess-concentration;
ΔC	= time-mean excess-concentration;
f_o	= occuring frequency of initial instability;
$f(t)$	= similarity function regarding $U(y,z)$;
Fd	= densimetric Froude number;
g	= constant gravitational acceleration;

$g(t)$ = similarity function regarding ΔC;

H_o = depth at the outfall;

H_e, H_n, H_R = jet depths;

Q = total volume flux along x;

Q_E, Q_y, Q_z = entrained volume flux;

L_o, L_E = length from the outfall;

Ri = local Richardson number;

$\overline{Ri}$ = overall Richardson number;

St_o = Strouhal number of initial instability;

u_f = front velocity of buoyant discharge along y;

u_x = convective velocity of buoyant discharge along x;

u' = rms value of fluctuating longitudinal velocity;

U = time-mean longitudinal velocity;

V_E, $\hat{V}_E$ = lateral entrainment velocity;

$\tilde{V}_E$ = entrainment velocity perpendicular to the jet boundary;

V_{ap} = convective velocity of particle toward the jet boundary;

W_E = vertical entrainment velocity;

x = longitudinal coordinate taken along the main flow direction;

y = lateral coordinate;

z = vertical coordinate;

α_y, α_z, α_E = entrainment constants ($\alpha_y = V_E/U_s$);

β = constant;

θ = right angle of convective velocity V_{ap} with jet axis;

ε = relative density difference ($\varepsilon = \Delta\rho/\rho_a$);

ρ = density of fluid;

ρ_a = density of ambient fluid;

$\Delta\rho$ = density difference ($\Delta\rho = \rho - \rho_a$); and

ν = kinematic viscosity.

Subscripts :

e = depth or width defined as $U = U_s/2.718$;

E = entrainment;

n = depth or width of nominal boundary;

o = conditions at the outfall; and

s = water surface on the jet axis.